creative commons
COMMONS DEED

저작자표시-비영리-동일조건변경허락 2.0 대한민국

이용자는 아래의 조건을 따르는 경우에 한하여 자유롭게

- 이 저작물을 복제, 배포, 전송, 전시, 공연 및 방송할 수 있습니다.
- 이차적 저작물을 작성할 수 있습니다.

다음과 같은 조건을 따라야 합니다:

저작자표시. 귀하는 원저작자를 표시하여야 합니다.

비영리. 귀하는 이 저작물을 영리 목적으로 이용할 수 없습니다.

동일조건변경허락. 귀하가 이 저작물을 개작, 변형 또는 가공했을 경우에는, 이 저작물과 동일한 이용허락조건하에서만 배포할 수 있습니다.

- 귀하는, 이 저작물의 재이용이나 배포의 경우, 이 저작물에 적용된 이용허락조건을 명확하게 나타내어야 합니다.
- 저작권자로부터 별도의 허가를 받으면 이러한 조건들은 적용되지 않습니다.

저작권법에 따른 이용자의 권리는 위의 내용에 의하여 영향을 받지 않습니다.

이것은 이용허락규약(Legal Code)을 이해하기 쉽게 요약한 것입니다.

Disclaimer

dCollection

공학석사 학위논문

Hydrothermal Synthesis of Branched ZnO Nanowire Array as an Effective Photoanode for Quantum-Dot-Sensitized Solar Cells

수열 합성을 통한 산화아연 브랜치 나노와이어의 양자점 감응형 태양전지 광전극으로의 활용

2014년 2월

서울대학교 대학원
재료공학부
강 수 지

Hydrothermal Synthesis of Branched ZnO Nanowire Array as an Effective Photoanode for Quantum-Dot-Sensitized Solar Cells

수열 합성을 통한 산화아연 브랜치 나노와이어의 양자점 감응형 태양전지 광전극으로의 활용

지도교수 박 병 우

이 논문을 공학석사 학위논문으로 제출함.
2014년 2월

서울대학교 대학원
재료공학부
강 수 지

강수지의 공학석사 학위논문을 인준함.

2014년 2월

위 원 장 강 신 후
부위원장 박 병 우
위 원 박 찬

Abstract

I have focused on the synthesis of branched ZnO nanowires and the understanding of the growth kinetics during my thesis. Furthermore, the branched ZnO nanowire array was introduced as a photoelectrode of a quantum-dot-sensitized solar cell, and the correlation between the nanostructures and solar cell performance was investigated in terms of both optical (light trapping) and electrical (charge recombination) characteristics.

Three-dimensional branched ZnO nanowires were synthesized by a seed-mediated hydrothermal growth. The fast growth-rate of (001) direction was possible due to the anisotropic nature of ZnO and the capping agents blocking a lateral growth of nanowire.

About two-fold enhancement of power conversion efficiency (PCE) was obtained by growing secondary branches, and both short-circuit current and open-circuit voltage were enhanced. Highly increased surface area of photoelectrode, resulting in higher light harvesting from increased quantum-dot loading amount, and the higher diffused reflectance was observed due to enhanced light-scattering of 3D structure. In addition, electrochemical impedance spectroscopy and open-circuit voltage decay revealed the reduced recombination and higher lifetime of branched ZnO nanowires.

Keywords: Quantum-dot-sensitized solar cell, Zinc oxide, Nanowire array, Hierarchical structure, Light trapping

Student Number: 2012-20573

Table of Contents

List of Figures

Chapter 1.

Chapter 2.

List of Table

Chapter 2.

Chapter 1. Overview

1.1 Quantum-Dot-Sensitized Solar Cells

1.1.1 General Introduction to Quantum-Dot-Sensitized Solar Cells

As solar cells emerge as the next-generation energy devices, single-crystalline silicon solar cells with high efficiency (~25%) have been already invented and commercialized. However, the high cost of manufacturing processes is a main obstacle for a wide application.

To overcome this, potential alternative solar cells have been researched, and Grätzel and O'Regan designed the dye-sensitized mesoporous TiO_2 structure in 1991, which achieved ~7 % of the power-conversion efficiency [1]. This structure has been paid attention due to its lower manufacturing cost and relatively high efficiency, whereas quantum-dot-sensitized solar cells (QDSCs) have been also attracted using semiconductor-quantum dots as light-absorbing materials, which have advantages over dye-sensitized solar cells (DSSCs).

First, Quantum dots have higher absorption coefficients (10^5 - 10^6 / M·cm) compared to dye molecules [2], which assures effective utilization of incident solar light.

Second, the absorption of quantum dots can be tailored via control of their size due to a quantum-size effect [3]. Moreover, it was found that the multiple-exciton generation is also possible by absorbing photons with the higher energy than the band gap of quantum dots, and this implies the possibility of exceeding the Schottky-Queisser limit [4].

With all these advantages, the state-of-art QDSCs achieved high efficiencies over

5% [5], and X. Zhong's group reported $CdSe_xTe_{1-x}$ alloyed QDSC with power conversion efficiency exceeding 6% [6]. It is believed QDSCs are highly promising candidate for a next major solar cell kind.

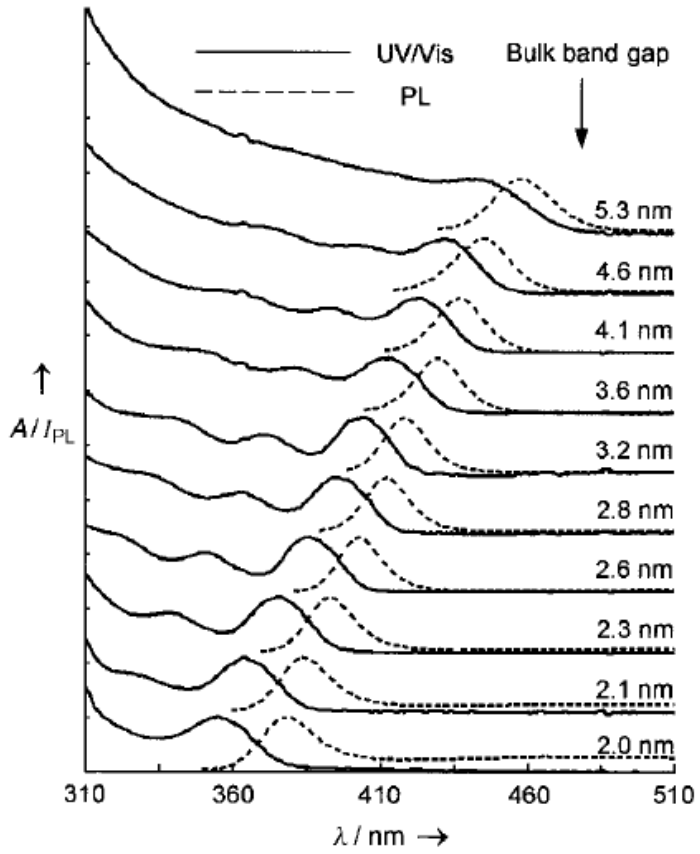

Fig.1-1. UV/Vis absorption and photoluminescence (PL) spectra of the CdS nanocrystals with different sizes [3].

1.1.2 Principles of Quantum-Dot-Sensitized Solar Cells

A quantum-dot-sensitized solar cell consists of working electrode, counter electrode, and electrolyte. The working electrode is composed of wide-band gap semiconductor as an electron conductor on transparent conducting electrode (TCO), and quantum dots as light-absorber materials.

Under illumination of AM 1.5G, a standard solar spectrum, QDs absorb photons with the energy higher than that of band gap, and excited electrons are injected into wide-band gap semiconductor and captured by TCO. Holes generated in QDs are scavenged by redox couples in electrolyte, such as polysulfide (S^{2-}/S_x^{2-}), and finally the oxidized species (S^{2-}) is reduced on the counter electrode [7]. This is the working principle of QDSCs under irradiation of sunlight and illustrated in Fig. 1-2.

For QDSCs, trap states exist not only in wide band gap semiconductors but also in QDs, resulting in different charge transfer and recombination process from DSSCs. Electrons in oxide semiconductor can be trapped at defect states and can be recombined with holes in the electrolyte, so negative backward recombination is more severe than DSSCs.

The power conversion efficiency (η) of QDSC can be calculated from current density-voltage (*J*-*V*) curves, according to the equation,

$$\eta = \frac{V_{OC} J_{SC} FF}{P_{in}}$$

Where V_{OC} is open-circuit voltage, J_{SC} is short-circuit current, *FF* is a fill factor, and P_{in} is incident power. V_{OC} is the maximum voltage when current is zero due to same

rate of excitation and recombination of electrons, and its upper limit is determined from the difference between conduction-band edge of semiconductor and potential of the electrolyte [8]. J_{SC} is the maximum current when applied voltage is zero, and it's related to light absorbing and charge collection of photoelectrode. *FF* is defined as the ratio of ($V_{max} \times J_{max}$) to ($V_{OC} \times J_{SC}$), and its value is lower than that of ideal *J-V* curve due to the existence of the series and shunt resistances in the cell [7]. The series resistances are from transport, interface, and diffusion resistances, and the shunt resistances are related to the recombinations at semiconductor/electrolyte and TCO/electrolyte interfaces, which lowers J_{SC} as well as V_{OC}. To achieve highly efficient solar cells, the lower the series resistance, and the higher the shunt resistance are required.

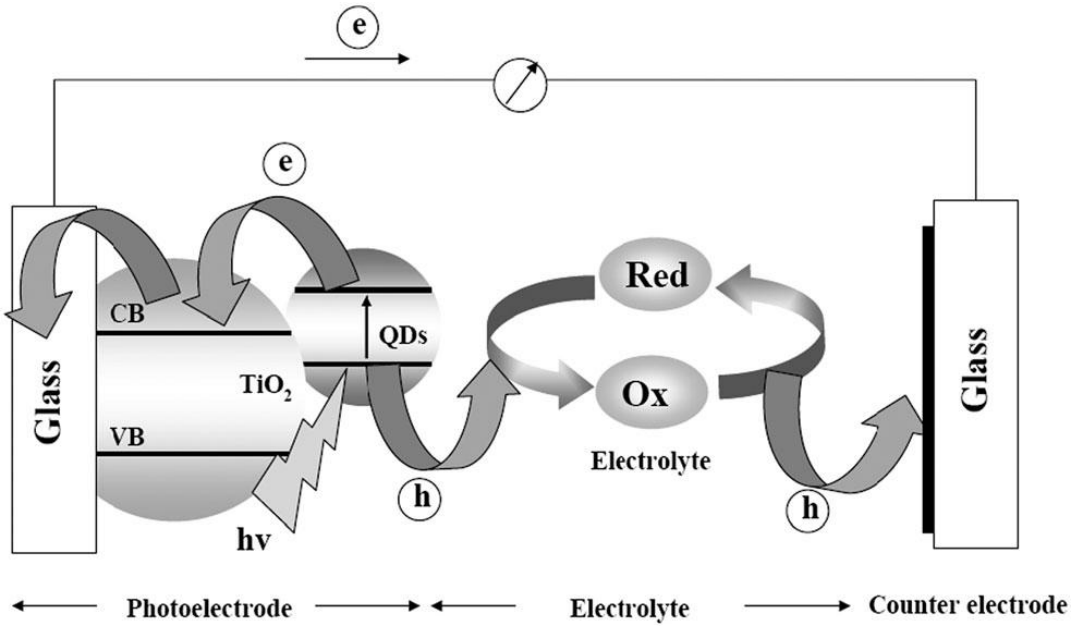

Fig. 1-2. Operating principle of a typical QDSC [7].

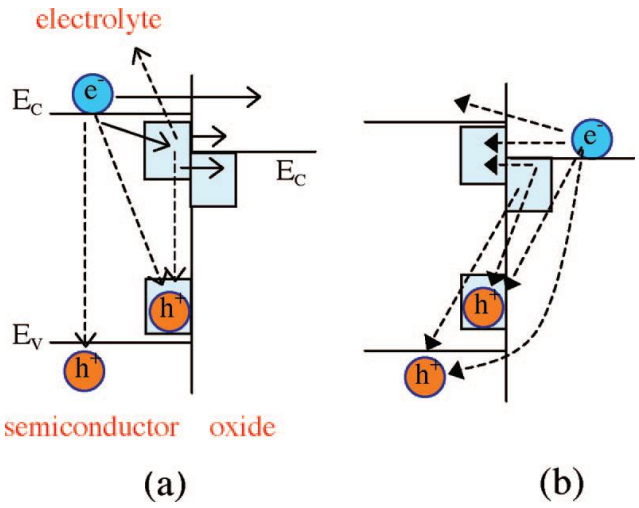

Fig. 1-3. (Color) Schematic diagrams of electron transfer processes for electrons in the semiconductor (a) and from the oxide to the semiconductor (b) [9]

1.2 Zinc Oxide as a Photoelectrode Material

1.2.1 Advantages of ZnO as a photoelectrode material

In dye-sensitized solar cells and quantum-dot-sensitized solar cells, as third-generation photoelectrochemical (PEC) cells, which work differently from Si-based solar cells, exciton generation and charge transfer occur separately at light absorber and oxide-semiconductor photoelectrode, respectively. As the main role of the semiconductor material is conduction of injected electrons, conduction-band edge should be located at proper position for injection of excited electrons of light absorbers and sufficient V_{OC}. Among the various wide-band gap oxide semiconductors, TiO_2 and ZnO have proper band alignment which are similar with each other [10], and have been the most widely researched as photoelectrode materials.

In addition, the breakthrough of the low power conversion efficiency of DSSCs was achieved from the introduction of connected TiO_2 nanoparticles as a photoelectrode due to an enormous increase in internal surface area, leading to increase of dye loading [1]. The nanostructure of photoelectrode is highly important in terms of the internal surface area for loading of light-absorber materials, and ZnO material is versatile to form various effective nanostructures compared to TiO_2.

ZnO, an attractive photoelectrode material, is known to be wurtzite structure under a conventional condition, and it has a hexagonal unit cell with the space group C6mc with the lattice parameters of a = 0.329 nm, and c = 0.5207 nm. The asymmetry of wurtzite structure as well as $\pm$(0001) polar surfaces leads to an easy anisotropic growth due to the difference of crystallographic plane surface energies and polarities [11].

Because of the easy anisotropic growth of ZnO material, a wide variety of nanostructures can be synthesized, such as ZnO nanoparticles, one-dimensional (1D) nanowires/rods/tubes/fibers, 2D nanosheets/belts/plates, and 3D hierarchical structures via various techniques including thermal evaporation, dc plasma reaction, chemical vapor deposition (CVD), molecular beam epitaxy (MBE), sputtering, and solution-derived synthesis methods, etc. [12].

Further, the single-crystal ZnO has carrier mobility (115 - 155 cm^2/Vs) [13], which is 2 orders of magnitude higher than that of TiO_2 (1 - 4 cm^2/Vs) [14], indicating much faster electron transport.

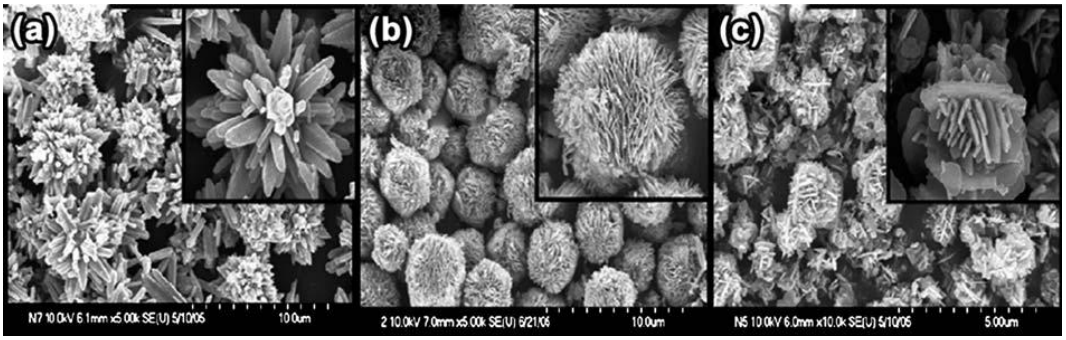

Fig. 1-4. SEM images showing various ZnO nanostructures. (a) Nnanoflowers. (b) Nanosheet spheres. (c) Nanoplate aggregates [11].

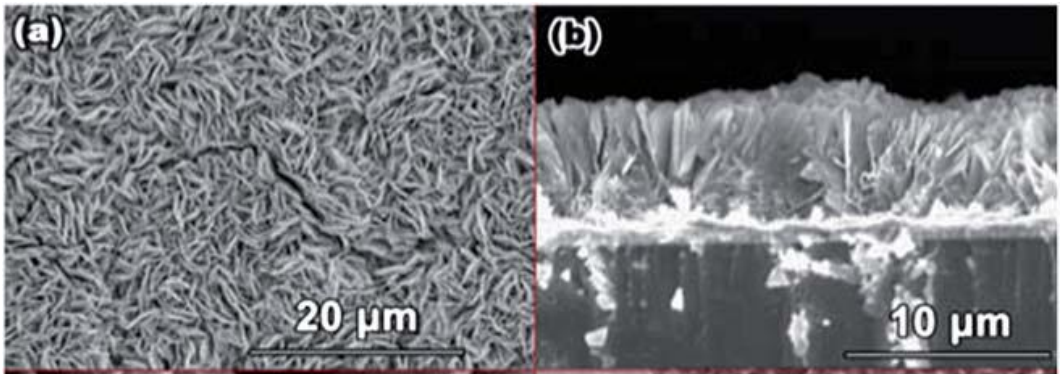

Fig. 1-5. SEM images of the ZnO nanosheet arrays derived from a CBD method [11].

1.2.2 One-dimensional ZnO nanostructure

By introducing photoelectrode consists of nanocrytalline TiO_2, the breakthrough was achieved in PCE due to an increase in surface area, and nanocrytalline TiO_2 have been widely used in DSSCs and QDSCs. However, this structure has severe drawbacks in electron transfer because of trapping occurs at numerous grain boundaries in nanoparticulate film, which indicates extremely slow nature of electron transfer. In addition, a drift transport, which is critical mechanism in photovoltaic cells, is also inhibited by discontinuity of electrostatic potential due to the mesoporous structure [15]. One-dimensional structure grown vertically on transparent conducting oxide is attractable with its superior electron transport.

Due to an anisotropic-growth characteristic of ZnO, 1D nanowire/nanorod/nanotube structures are obtained via physical vapor deposition, electrochemical deposition, hydrothermal method etc. [16], and P. Yang's group reported ZnO nanowire array by hydrothermal growth as a photoelectrode of a DSSC, which consumes low energy and environmentally benign method [15]. ZnO nanowires with a high aspect ratio of ~125 and the length of 25 μm attained high density and sufficient surface area. Large electron diffusion coefficients (0.05 - 0.5 /cm^2 s) of single nanowires were obtained and are about 3 orders of magnitude higher than those of nanoparticulate films (10^{-5} - 10^{-4} /cm^2 s) [17,18].

The insufficiency of surface area for photoelectrode can be overcome by longer diffusion length. Superior charge collection of ZnO nanowire was observed in comparison of J_{SC} with ZnO nanoparticulate electrode with the same amount of dye

loading, and this is explained as radial and axial electric fields assist electron transport toward external circuits [15].

Since the report of P. Yang's group, ~7% of PCE is achieved in DSSCs [19], and K. Yong's group reported the PCE of 4.15 % with the CdS/CdSe co-sensitized solar cell [20].

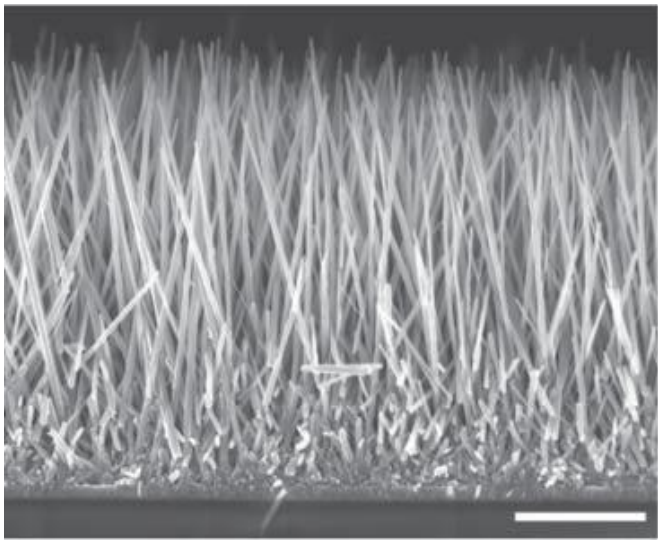

Fig. 1-6. SEM image of the hydrothermally grown ZnO nanowire array on TCO. Scale bar, 5 μm [15].

1.2.3 Hierarchical ZnO Structures

Hierarchical structures (HS) or superstructures involve substructures and demonstrate dual or even multiple functions depend on their shape and size [21]. These structures enable remarkable performances of energy storage/generating devices, especially PEC cells. Submicron or micron dimension can operate as light-scattering centers or rapid pathway of electrons, and nano-dimension substructure can ensure large internal surface area.

Various ZnO HSs are synthesized and adopted for photoelectrode DSSCs and QDSCs. First, hierarchical spheres consisting nanoparticles or nanowires/rods are synthesized by hydrothermal method. In the previous studies, to enhance the optical path length, submicron spheres of which the size is comparable to the wavelength of visible light were added in nanoparticulate electrode, however, the loss of surface area causes degradation of cell performance due to the decreased dye loading. HS sphere effectively enhances the light scattering as well as electrolyte wetting by provide larger pores and at the same time ensures the sufficient surface area. Since G. Cao's group reported high PCE of DSSC with ZnO aggregates, which is 5.4% of PCE compared to 2.4% of ZnO-nanocrystalline DSSC, this structure has been paid attention to as an effective morphology for a photoelectrode [22].

Second, 3D branched nanowire structures with high surface area and direct transport pathway are also emerging as photoelectrode. Nanowire array shows excellent electron transport, but suffers from insufficient internal surface area compared to nanoparticulate film. This weakness is crucial for high PCE, so hierarchical-nanowire

morphology is suggested for multiple functions, such as electron path way, higher surface area, and enhanced light scattering. Based on ZnO nanowires vertically grown on TCO as a backbone structure, secondary nanowires [23,24] or nanosheets [25,26] are deposited onto the backbones, or nanoparticles are included in the voids between nanowires [27]. Hydrothermally grown 3D branched ZnO nanowire array was used as a photoelectrode of DSSC by W. -F. Hsieh's group [23], and S. Ko's group reported about 4-fold increase in PCE with branched nanowire array [24]. Si nanowire based ZnO-branched QDSC was also reported and showed V_{OC} as high as 0.77 V [28].

Furthermore, tetrapod, plate and fiber based 3D HSs [29-31] are synthesized with ZnO and introduced to DSSCs and QDSCs.

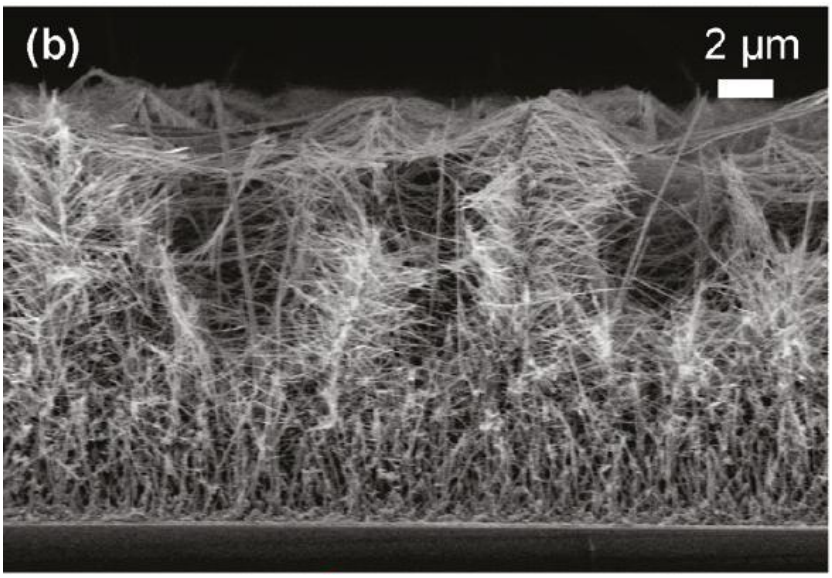

Fig. 1-7. Cross-sectional SEM image of the branched ZnO nanowire array [24].

1.3 References

1. B. O'Regan and M. Grätzel, "A Low-Cost, High-Efficiency Solar Cell Based on Dye-Sensitized Colloidal TiO_2 Films," *Nature* **353**, 737 (1991).
2. U. R. Genger, M. Grabolle, S. C. Jaricot, R. Nitschke, and T. Nann, "Quantum Dots versus Organic Dyes as Fluorescent Labels," *Nat. Methods* **5**, 9 (2008).
3. W. Yu and X. Peng, "Formation of High-Quality CdS and Other II-VI Semi conductor Nanocrystals in Noncoordinating Solvents: Tunable Reactivity of M onomers," *Angew. Chem. Int. Ed.* **41**, 2368 (2002).
4. R. J. Ellingson, M. C. Beard, J. C. Johnson, P. Yu, O. I. Micic, A. J. Nozik, A. Shabaev, and A. L. Efros, "Highly Efficient Multiple Exciton Generation in Colloidal PbSe and PbS Quantum Dots," *Nano Lett.* **5**, 865 (2005).
5. J. -W. Lee, D. -Y. Son, T. K. Ahn, H. -W. Shin, I Y Kim, S. -J. Hwang, M. J. Ko, S. Sul, H. Han, and N. -G. Park, "Quantum-Dot-Sensitized Solar Cell with Unprecedentedly High Photocurrent," *Science Rep.* **3**, 1050 (2013).
6. Z. Pan, K. Zhao, J. Wang, H. Zhang, Y. Feng, and X. Zhong, "Near Infrared Absorption of $CdSe_xTe_{1-x}$ Alloyed Quantum Dot Sensitized Solar Cells with More than 6% Efficiency and High Stability," *ACS Nano* **7**, 5215 (2013)
7. Z. Yang, C. -Y. Chen, P. Roy, and H.-T. Chang, "Quantum Dot-Sensitized Solar Cells Incorporating Nanomaterials," *Chem. Commun.* **47**, 9561 (2011).
8. S. Ruhle, M. Shalom, and A. Zaban, "Quantum-Dot-Sensitized Solar Cells," *ChemPhysChem.* **11**, 2290 (2010).
9. G. Hodes, "Comparison of Dye- and Semiconductor-Sensitized Porous

Nanocrystalline Liquid Junction Solar Cells," *J. Phys. Chem. C* **112**, 17778 (2008).

10. K. Kalyanasundaram and M. Grätzel, "Applications of Functionalized Transition Metal Complexes in Photonic and Optoelectronic Devices," *Coord. Chem. Rev.* **248**, 1181 (2004).
11. F. Xu and L. Sun, "Solution-Derived ZnO Nanostructures for Photoanodes of Dye-Sensitized Solar Cells," *Energy Environ. Sci.* **4**, 818 (2011).
12. Z. L. Wang, "Zinc Oxide Nanostructures: Growth, Properties and Applications," *J. Phys.: Condens. Matter* **16**, R829 (2004).
13. E. M. Kaidashev, M. Lorenz, H. Von Wenckstern, A. Rahm, H. C.Semmelhack, K.-H. Han, G. Benndorf, C. Bundesmann, H. Hochmuth, and M.Grundmann, "High Electron Mobility of Epitaxial ZnO Thin Films on C-plane Sapphire Grown by Multistep Pulsed-Laser Deposition," *Appl. Phys. Lett.* **82**, 3901 (2003)
14. K. Tang, R. Prasad, P. E. Sanjinès, and F. Lévy, "Electrical and Optical Properties of TiO_2 Anatase Thin Films," *J. Appl. Phys.* **75**, 2042 (1994)
15. M. Law, L. E. Greene, J. C. Johnson, R. Saykally, and P. Yang, "Nanowire Dye-Sensitized Solar Cells," *Nat. Mater.* **4**, 455 (2005).
16. L. Lin, T. Zhain, Y. Bando, and D. Golberg, "Recent Progress of One-dimensional ZnO Nanostructured Solar Cells," *Nano Energy* **1**, 912 (2012).
17. N. Kopidakis, K. D. Benkstein, J. Lagemaat, and A. J. Frank, "Transport-Limited Recombination of Photocarriers in Dye-Sensitized Nanocrystalline TiO_2 Solar Cells ," *J. Phys. Chem. B* **107**, 11307 (2003).
18. V. Noack, H. Weller, and A. Eychmüller, "Electron Transport in Particulate ZnO

Electrodes: a Simple Approach," *J. Phys. Chem. B* **106**, 8514 (2002).

19. L. -Y. Chen and Y. -T. Yin, "Hierarchically Assembled ZnO Nanoparticles on High Diffusion Coefficient ZnO Nanowire Arrays for High Efficiency Dye-Sensitized Solar Cells," *Nanoscale* **5**, 1777 (2013).
20. M. Seol, H. Kim, Y. Tak and K. Yong, "Novel Nanowire Array Based Highly Efficient Quantum Dot Sensitized Solar Cell," *Chem. Commun.* **46**, 5521 (2010).
21. Y. Shi, C. Zhu, L. Wang, C. Zhao, W. Li, K. K. Fung, T. Ma, A. Hagfeldt, and N. Wang, "Ultrarapid Sonochemical Synthesis of ZnO Hierarchical Structures: From Fundamental Research to High Efficiencies up to 6.42% for Quasi-Solid Dye-Sensitized Solar Cells," *Chem. Mater.* **25**, 1000 (2013).
22. Q. Zhang, T. P. Chou, B. Russo, S. A. Jenekhe, and G. Cao, "Aggregation of ZnO Nanocrystallites for High Conversion Efficiency in Dye-Sensitized Solar Cells," *Angew. Chem.* **120**, 2436 (2008).
23. H. -M. Cheng, W. -H. Chiu, C. -H. Lee, S. -Y. Tsai, and W. -F. Hsieh, "Formation of Branched ZnO Nanowires from Solvothermal Method and Dye-Sensitized Solar Cells Applications," J. Phys. Chem. C 112, 16359 (2008).
23. S. H. Ko, D. Lee, H. W. Kang, K. H. Nam, J. Y. Yeo, S. J. Hong, C. P. Grigoropoulos, and H. J. Sung, "Nanoforest of Hydrothermally Grown Hierarchical ZnO Nanowires for a High Efficiency Dye-Sensitized Solar Cell," *Nano Lett.* **11**, 666 (2011).
25. S. Zhu, L. Shan, X. Chen, L. He, J. Chen, M. Jiang, X. Xieab, and Z. Zhou, "Hierarchical ZnO Architectures Consisting of Nanorods and Nanosheets Prepared

via a Solution Route for Photovoltaic Enhancement in Dye-Sensitized Solar Cells," *RSC Advances* **3**, 2910 (2013).

26. H. Kim and K. Yong, "A Highly Efficient Light Capturing 2D (Nanosheet)-1D (Nanorod) Combined Hierarchical ZnO Nanostructure for Efficient Quantum Dot Sensitized Solar Cells," *Phys. Chem. Chem. Phys.* **15**, 2109 (2013).
27. C. -T. Wu, W. -P. Liao, and J. -J. Wu, "Three-Dimensional ZnO Nanodendrite/Nanoparticle Composite Solar Cells," *J. Mater. Chem.* **21**, 2871 (2011).
28. P. Sudhagar, T. Song, D. H. Lee, I. Mora-Seró, J. Bisquert, M. Laudenslager, W. M. Sigmund, W. I. Park, U. Paik, and Y. S. Kang, "High Open Circuit Voltage Quantum Dot Sensitized Solar Cells Manufactured with ZnO Nanowire Arrays and Si/ZnO Branched Hierarchical Structures," *J. Phys. Chem. Lett.* **2**, 1984 (2011).
29. Z. Zhu, J. Qiu, K. Yan, and S. Yang, "Building High-Efficiency CdS/CdSe-Sensitized Solar Cells with a Hierarchically Branched Double-Layer Architecture," *ACS Appl. Mater. Interfaces.* **5**, 4000 (2013).
30. M. McCune, W. Zhang, and Y. Deng, "High Efficiency Dye-Sensitized Solar Cells Based on Three-Dimensional Multilayered ZnO Nanowire Arrays with "Caterpillarlike"Structure," *Nano Lett.* **12**, 3656 (2012).
31. H. Chen, W. Li, H. Liu, and L. Zhu, "CdS Quantum Dots Sensitized Single- and Multi-layer Porous ZnO Nanosheets for Quantum Dots-Sensitized Solar Cells," *Electrochem. Comm.* **13**, 331 (2011).

Chapter 2.

Hydrothermal Synthesis of Branched ZnO Nanowire Array as an Effective Photoanode for Quantum-Dot-Sensitized Solar Cells.

2.1 Introduction

Quantum-dot-sensitized solar cells (QDSC) have been paid considerable attention to as the next-generation solar cells. By adopting quantum dots (QD) with unique physical properties as light absorbing materials for photovoltaic devices, exceptional advantages are expected. First, due to the quantum confinement effect, light absorption can be tailored by simply changing the size of QDs. Secondly, QDs have higher molar absorption coefficient (10^5 - 10^6 /M cm) than that of dyes (10^4 - 10^5 /M cm) for dye-sensitized solar cells (DSSC) [1]. Moreover, multiple-exciton generation by impact ionization is reported, indicating the possibility of the high power conversion efficiencies exceeding the theoretical limit [2].

A TiO_2 mesoporous film has been the most extensively used as a photoelectrode of QDSCs, however, numerous grain boundaries act as trap sites during electron transfer, resulting in the slow nature of transport [3]. ZnO is another oxide of which band-gap energy is close to that of TiO_2, and due to its higher carrier mobility than that of TiO_2 [4] and easy anistropic crystallization [5], it has been also widely utilized as a photoelecrode material of QDSCs in forms of various nanostructures including nanowires, nanosheets, nanoaggregates, and etc..

One-dimensional (1D) ZnO nanowire array vertically grown on transparent

conducting oxide is one of the most attractive nanostructures. This structure provides not only a direct pathway for electron conduction but also internal electric field which supports collection of electrons. Electron transport is superior to mesoporous structures, but internal surface area is insufficient for QD loading, which is the major drawback of 1D nanostructure [3].

Three-dimensional hierarchical structure consisting of substructures serves double or multiple functions to give high performance of photovoltaic devices [6]. 1D-nanowire-based 3D-hierarchical structure provides fast electron transfer, and substructures, such as, secondary nanowires, nanosheets, and nanoparticles, effectively increase the internal surface area. In this regard, 3D ZnO hierarchical structures have been introduced for photoelectrodes of DSSCs, and the impressive enhancements of PCE were observed [7-9]. Recently, there have been a few attempts to apply 3D-hierarchical nanostructures to QDSCs owing to their remarkable usability as a photoelectrode, however, the obtained 3D morphologies have sparse substructures, leaving a room for the additional increase of surface area for higher QD loading [10,11].

In this study, 3D-branched ZnO nanowire arrays are introduced as that of the QDSC. The primary nanowires which involve secondary 1D-branches were synthesized via simply repeating the same hydrothermal growth, which is known to be low-energy consuming and environment-benign process. Compared to the other 3D ZnO hierarchical structures, the substructures themselves are also 1D nanowires which can play important roles in increasing internal surface area, acting as direct pathways for electron transfer, and enhancing the light scattering and capturing. As mentioned

above, this structure was already adopted for DSSCs, however, it is the first try to utilize this nanostructure for a photoelectrode of QDSC, and observe the effect of branches on the light harvesting and the cell performance of QDSC.

2.2 Experimental Section

ZnO Nanowire Array Growth

Fluorine-doped tin oxide substrates (FTO, TEC 8: Pilkington) were served as substrates. For the TiO_2 blocking layer, pure $TiCl_4$ was added to pre-cooled (~0℃) deionized H_2O to make a 40 mM $TiCl_4$ aqueous solution, and the substrates were dipped in the solution for 30 min at 70℃, followed by annealing at 450℃ for 30 min under air.

For hydrothermal ZnO-nanowire growth, the D. Gao group's method was adopted [12]. First, ZnO seeds were grown on the $TiCl_4$-treated FTO, for which 0.5 mM zinc acetate dihydrate ($Zn(CH_3COO)_2$ $2H_2O$) ethanol solution of 50 μL was dropped on the substrate and, spin-coated with 3000 rpm for 30 s, and subsquently dried on a hot plate at 60℃. This procedure was repeated for 5 times, and finally the zinc acetate dihydrate was thermally decomposed by annealing under air at 400℃ for 1 h to make ZnO.

The seeded substrates were immersed in the aqueous solutions consisting of 25 mM of zinc nitrate hexahydrate, 25 mM of hexamethylenetetramine (HMTA), ammonium hydroxide (NH_4OH), and 2.5 mM poly(ethyleneimine) (PEI) in autoclaves. Hydrothermal syntheses were carried out at 95℃ for 8 h in the preheated oven. After the hydrothermal reaction, the ZnO-nanowire grown substrates were rinsed with ethanol and then dried at 60℃. To remove organic residues, heat treatments at 500℃ for 1 h under air were conducted.

Branched ZnO Nanowire Growth

ZnO branches were grown on the pre-grown nanowires by the same tactic. ZnO seeds were produced on the nanowires by thermal decomposition of zinc acetate layer formed from dip coating using a 5 mM zinc acetate solution in ethanol.

After thermal decomposition at 350℃ for 1 h, branch growth was carried out in the same solution at 95℃ for 3 h, and annealed at 500℃ for 1 h for organic removal.

Cell Fabrication

CdS QDs were coated on the branched ZnO nanowires by a successive ionic-layer adsorption and reaction (SILAR) method [13]. The as-prepared electrodes were soaked in a 0.04 M cadmium chloride ($CdCl_2$) dissolved in methanol for 1 min, and then were soaked in 0.04 M sodium sulfide (Na_2S) methanolic solution. Rinsing in methanol for 1 min and subsequent drying steps were also included between each immersion. The cycle was repeated for 9, 14, 20, 25 times.

Polysulfide electrolyte was prepared by dissolving 0.5 M Na_2S, 1 M S, and 0.02 M KCl in methanol/water solutions (7/3 volumic ratio) [14]. For a counter electrode, Ti was deposited on the pre-drilled FTO substrates as adhesion layer and Cu was deposited by rf magnetron sputtering. The Cu-deposited films were sulfurized in a polysulfide solution [15]. To fabricate sandwich-type solar cells, thermoplastic foil (60 μm; Dupont) was used as a spacer.

Characterizations

For the morphology observation of the branched ZnO nanowires, field-emission scanning electron microscopy (FE-SEM, JSM-6330F: JEOL) was used. X-ray diffraction (XRD, M18XHF-SRA: Mac Science) measurements were carried out for an the analyses of the crystalline structure. The photocurrent-voltage (*J*-*V*) curves were measured by the solar cell measurement system (K3000: McScience) with the solar simulator (Xenon lamp, air mass (AM) 1.5, 100 mW/cm^2). Impedance spectra and open-circuit decay curves were obtained using a potentiostat (CHI 604C: CH Instrumental Inc.). The absorbance and diffused reflectance spectra were recorded by a UV/Vis spectrophotometer (Cary 5000: Agilent Technologies).

2.3 Results and Discussion

Branched ZnO nanowre array on the FTO substrate were synthesized by repeating the hydrothermal growths, as shown in Fig. 2-1. The seed-mediated ZnO-branch growth method is adopted from W. -F. Hsieh's groups' method [7]. For the secondary branch-growth, nanowire-grown substrates were immersed in zinc acetate dihydrate solution, followed by drying procedure. While the immersion, zinc acetate dihydrates are adsorbed on the walls of primary ZnO nanowires, and ZnO seeds are obtained after thermal decomposition of zinc acetate dihydrate at 350℃. Secondary-seeded nanowire array went through another hydrothermal branch growth using the same aqueous solution for primary nanowire growth. By following relatively simple procedures using the same reagents for the different steps, hierarchical branched nanowires were obtained.

Scanning electron microscopy (SEM) images of ZnO nanowires and branched nanowires are shown in Fig. 2-2. Figure 2-2(a) shows cross-sectional ZnO nanowires, and the diameter and length of nanowires are 200 - 500 nm and ~8 μm, respectively. Figure 2-2(b) and (c) show branched ZnO nanowires and their magnified images. The length of branches is range from 1 to 2 μm, and the diameter is 20 - 30 nm. Random radial angles of branches from the primary nanowires indicate that branches are grown from individual ZnO nanocrystallites which we pre-coated, not the derivatives of the primary nanowires [7]. Branches are densely grown from the middle part of the primary nanowires, so voids between primary nanowires are filled with the branches, effectively enlarging the internal surface area. However, the bottom parts lack the

branches, leaving empty voids, probably due to the limited infiltration of seed precursors into the deep and narrow voids between primary nanowires [7]. For uniformly grown and denser branches, secondary seed-deposition condition needs further modification.

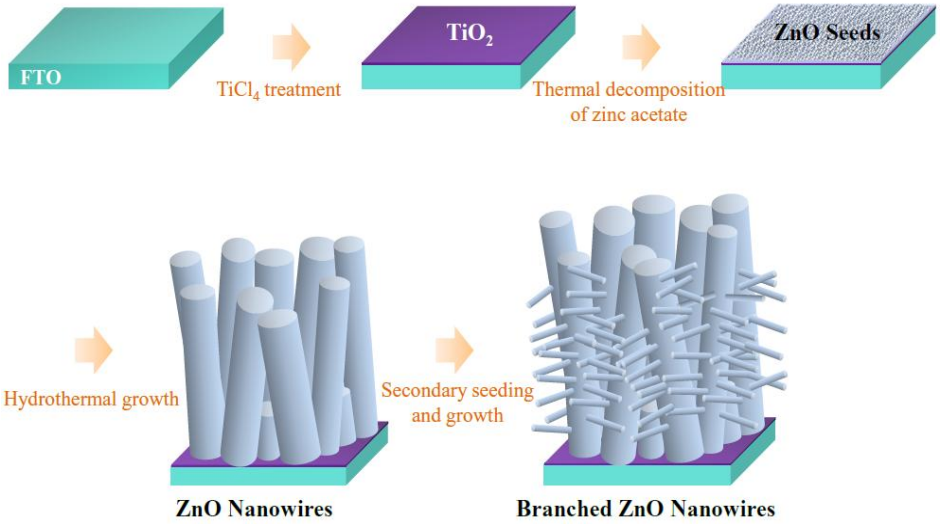

Fig. 2-1. (Color) A scheme showing synthetic of procedures for branched ZnO nanowires.

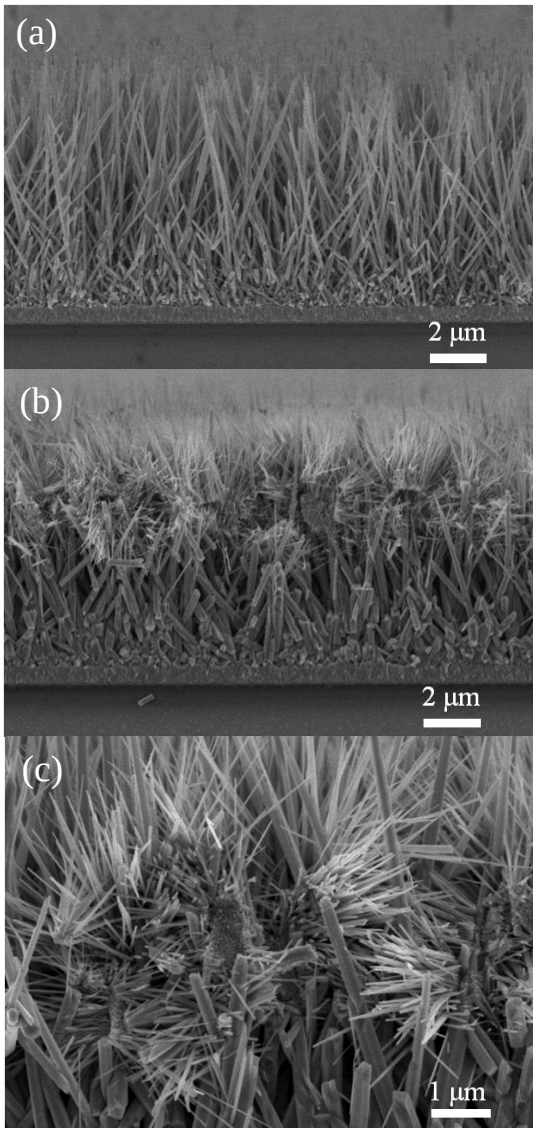

Fig. 2-2. Cross-sectional FE-SEM images of (a) the ZnO nanowires, (b,c) the branched ZnO nanowires.

Figure 2-3 displays x-ray diffraction patterns in logarithm scale of ZnO nanowires and branched nanowires grown on FTOs, and the crystalline structure of both nanostructures are characterized to be hexagonal wurtzite structure (JCPDS card No.36-1451) with no impurity peaks detected. The strong peaks of {0001} family indicate that the nanowire and branches oriented in the *c* axis direction. Hexagonal wurtzite ZnO has ±(0001) polar surfaces with alternating Zn^{2+}-terminated and O_2^--terminated surfaces, so incoming precursor molecules favorably absorb on the polar surface due to its high surface energy. After adsorption of whole layer of the precursors, the polarity inverts, and the oppositely charged precursors absorbed, causing fast crystal growth rate along the ±[0001] directions [16]. Polyethylenimine (PEI) was included in the growth solution as a capping agent which adsorbs onto the side surfaces and enhances the vertical growth. PEI is a nonpolar polymer which can be protonated over a wide range of pH values (pH 3 - 11) thereby positively charged. The isoelectric point of ZnO is at around pH = 9.5, so the sign of ZnO surface is negative above the isoelectric point, therefore electrostatic attraction drives PEI to be absorbed onto the side surfaces, leading to hinder the lateral growth [16].

We also observed that the sharper (100) and (110) peaks for the branched ZnO nanowires, which could be explained with the outward directions of branches from the primary nanowires. Compared to ZnO nanowire array, branched nanowires include branches with perpendicular *c* axis to that of primary nanowires, therefore, exposing (100) and (110) planes of branches parallel with (001) surfaces of primary nanowires.

On the other hand, branched ZnO nanowires showing a special orientation

relationship between primary nanowires are also reported [17]. In this case, independent ZnO seeds for the branch growth is not necessary, and zinc precursors are absorbed on the wall of primary nanowire with the least mismatch between primary nanowire. It is informed that [0001] and $[10\bar{1}1]$ directions in ZnO structure have ~5% lattice mismatch, which is the least, and consequentially, branches grown in [0001] direction are parallel with $[10\bar{1}1]$ direction of primary nanowire with the angle of 109.8° [17]. Figure 2-4 shows the atomic scale side-view and top-view of low-angle grain boundary of branched ZnO nanowire with the special oriental relationship.

To figure out the effect of 3D-branched morphology on the light absorption, the diffused reflectance and absorbance spectra are compared with the nanowire array. Fig. 2-5(a) is the diffused reflectance spectra of nanowire and branched nanowire before CdS QD sensitization. The branched nanowires exhibited higher diffused reflectance in the wavelength range from 400 to 800 nm, indicating that the branched ZnO nanowires have a higher light scattering ability than the nanowire sample, which can be helpful to utilize solar light by increasing optical path length. Absorbance spectra were also measured with CdS QD loading to examine the light-harvesting ability (Fig. 2-5(b)). The absorbance of branched nanowires is higher than that of nanowires from the wavelength of ~517 nm which is corresponding to CdS band gap of 2.4 eV [18]. It is believed that the more CdS QDs are loaded due to secondary branching.

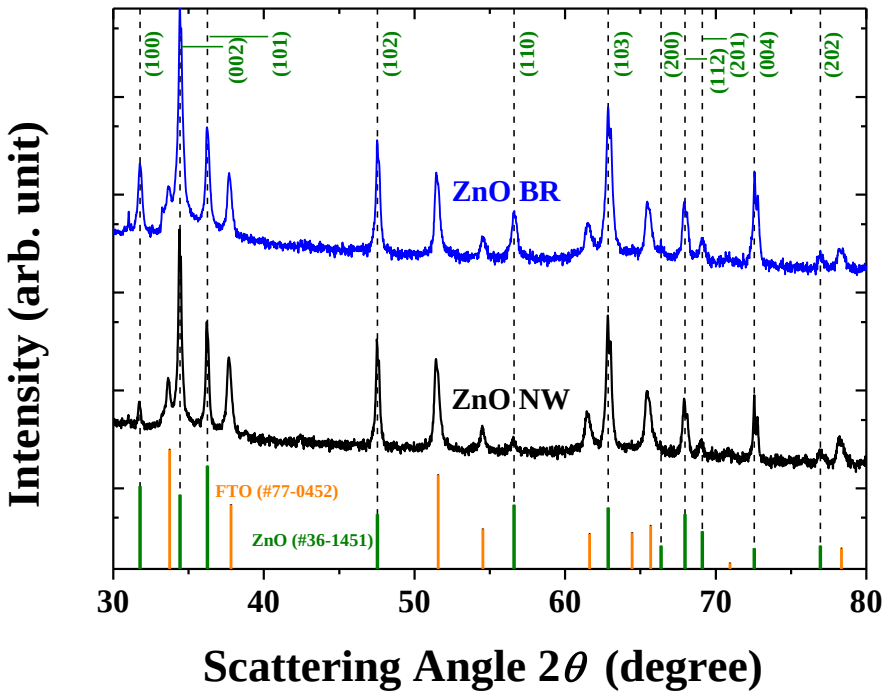

Fig. 2-3. (Color) X-ray diffraction patterns of the ZnO nanowires and the branched ZnO nanowires.

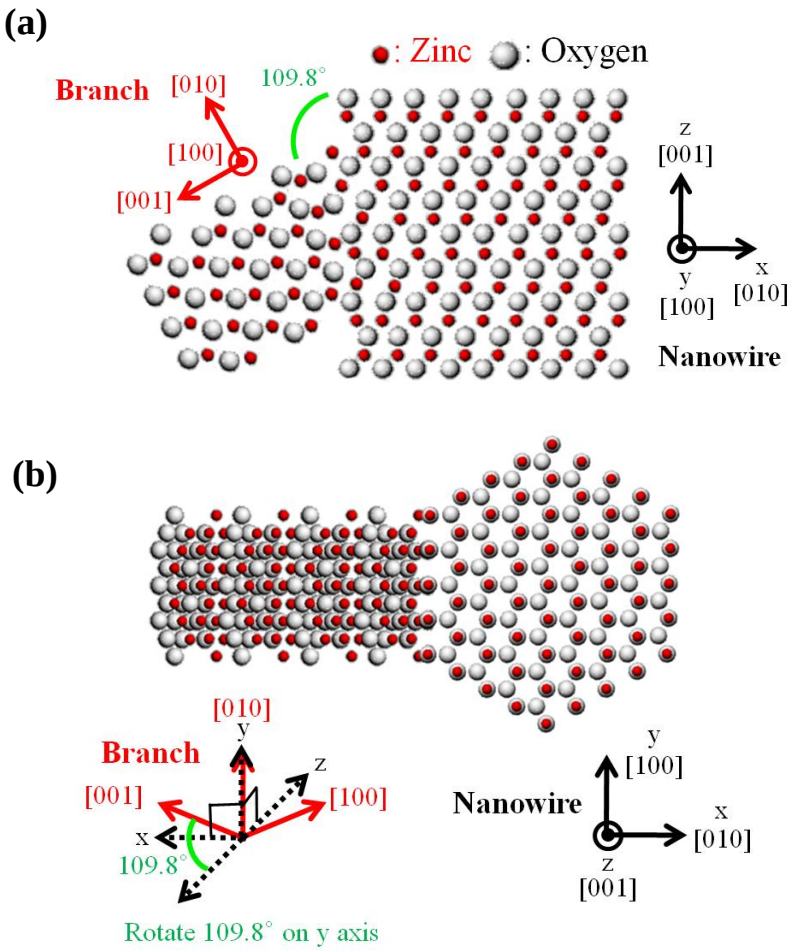

Fig. 2-4 (Color) Atomic scale (a) side-view and (b) top-view of branched ZnO nanowire with low-angle grain boundary. The angle between primary nanowire and branch is 109.8 ° [17].

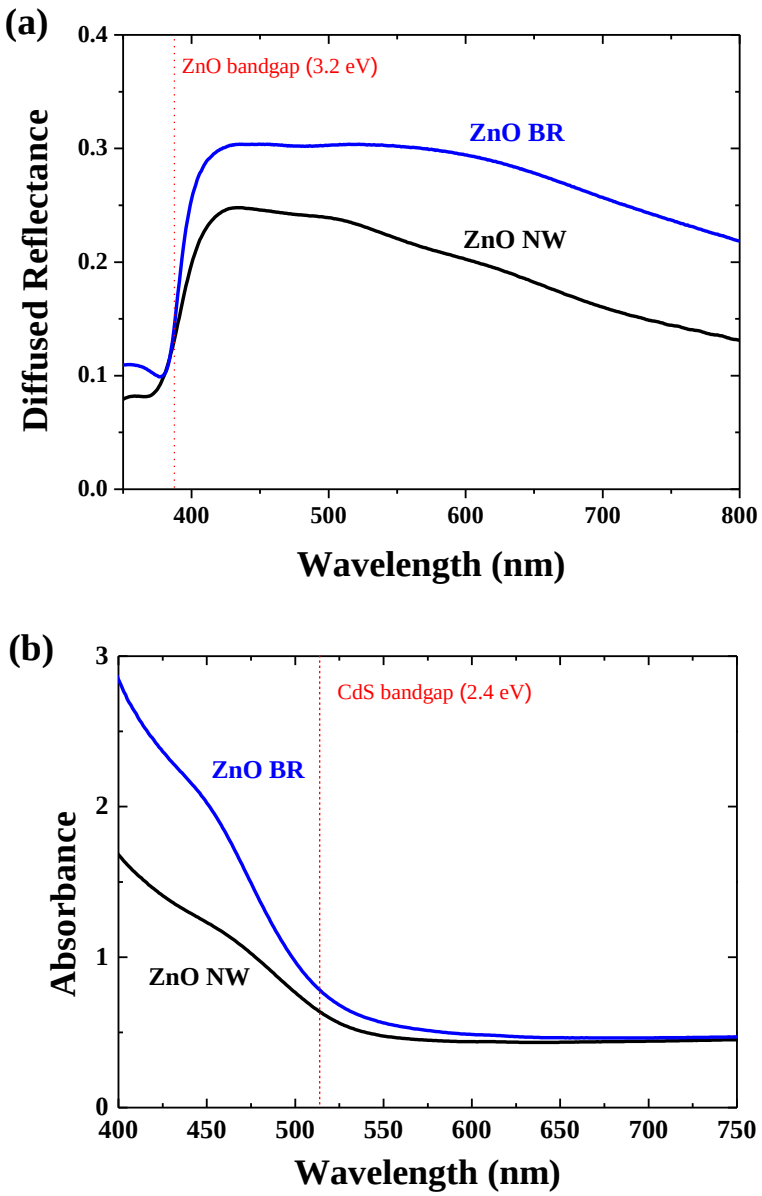

Fig. 2-5. (Color) Optical properties of the ZnO nanowire and the branched ZnO nanowires. (a) Diffused reflectance spectra before CdS sensitization. (b) Absorbance spectra after CdS sensitization.

From the *J-V* curves in Fig. 2-6, the branched ZnO structure with 9 SILAR cycles of CdS shows both improved short-circuit current (J_{SC}) and open-circuit voltage (V_{OC}), and the power conversion efficiency (PCE) achieved is 0.64% which is almost twice as that of nanowire array (0.37%). Fill factors are quiet similar to each other, and the obtained photovoltaic parameters are shown in Table 2-1. Dark currents were also measured, and the dark current of branched nanowires is lower than nanowires, indicating reduced back-transfer of electrons from ZnO to electrolyte, and this result is consistent with the higher V_{OC} of branched nanowires. More CdS SILAR cycles were performed to find the optimum cycle for the higher PCE, and 14, 20, 25 cycles were tried. Figure 2-7 shows the *J-V* curves with different SILAR cycles (9, 14, 20, 25), and 14-cycle sample showed the highest PCE of 1.5% with the highest J_{SC} and V_{OC}. As SILAR cycle increases, J_{SC} rapidly increased until 14 cycles and then dropped, however, V_{OC} and *FF* values were constantly decreased.

To further investigate the electrochemical reactions at the interfaces, electrical impedance spectroscopy (EIS) is utilized [19]. The measurement was carried out under AM 1.5 illumination (100 mW/cm^2) at open-circuit condition. At this condition, the transport resistance in ZnO nanowires is negligible, and the charge transfer at the ZnO/CdS/electrolyte interface is dominant [20]. Nyquist plot and Bode plot are obtained for branched nanowires and nanowires, as shown in Fig. 2-8. The charge transfer resistances were calculated by using equivalent-circuit model presented by Farbregat-Santiago *et al.* [20], and the corresponding equivalent circuit is shown in the inset of Fig. 2-8 [21]. R_S is a series resistance of FTO, and $R_{ZnO/CdS/el}$ means the charge-

transfer resistance for recombination from ZnO to CdS or electrolyte, and $C_{ZnO/CdS/el}$ means the capacitance at the ZnO/CdS/electrolyte interface. $Z_{d(el)}$ stands for the impedance of diffusion in the polysulfide electrolyte, and expressed as:

$$Z_{d(el)} = R \cdot \frac{\tanh(i\omega T)^P}{(i\omega T)^P} \quad (1)$$

where R is the diffusion resistance, ω is the angular frequency, T is a reciprocal of characteristic frequency of diffusion in a finite layer, and P is equal to 0.5 [22]. R_{Cu_2S} is the charge-transfer resistance from the electrolyte to Cu_2S counter electrode, and C_{Cu_2S} is the corresponding capacitance. The fitting lines are displayed in solid lines in Fig. 2-7, and the fitting parameters are listed in Table. 2-3.

Even though the ZnO/CdS/electrolyte interfaces are significantly increased by secondary branching, the charge transfer resistance is even increased. It could be indicated that the interfaces of branch/CdS/electrolyte do not suffer from the back recombination, further the charge transfer at the ZnO/CdS/electrolye is blocked by the secondary seeds coated onto the nanowires, resulting in higher V_{OC}. In other ZnO hierarchical structures which were previously reported, however, the charge transfer resistances are similar or even smaller for hierarchical structures due to the increased charge transfer interfaces [7,9]. Few studies reported for phase junction of hierarchical nanotrees and its effect on the electron transport [11]. So it would be worthwhile to investigate the ZnO/branch interface and branch/electrolyte interface charge transfers.

To further investigate the electron recombination characteristics of branched nanowires, the open-circuit voltage decay was observed and shown in Fig 2-9(a). The

open-circuit voltage decay rate is slower for the branched nanowires, which means the slower back recombination rate due to secondary branching. Therefore, more electrons are accumulated in branched ZnO nanowires, resulting in higher photovoltaic voltage [23].

The electron-carrier lifetime (τ) was calculated to quantify the V_{OC}-decay rate from the equation [24]:

$$\tau = -\frac{k_B T}{e}\left(\frac{dV_{oc}}{dt}\right)^{-1}. \quad (2)$$

$k_B T$ is the thermal energy and e is the elementary charge and dV_{OC}/dt is the derivative of V_{OC} with respect to time. The electron lifetime of the branched nanowires is higher at all voltages as shown in Fig 2-8(b), reassuring the hindered back recombination.

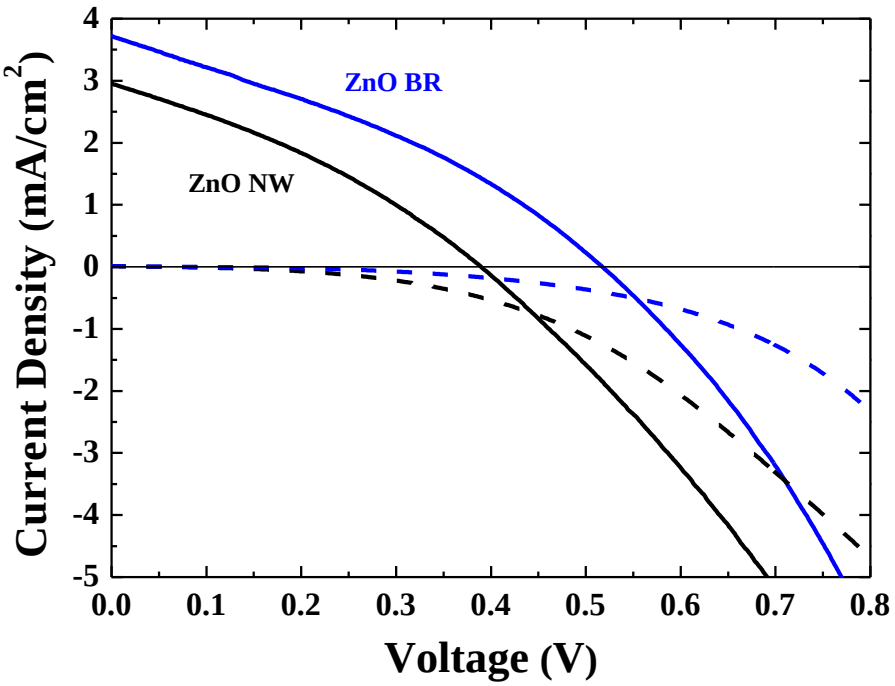

Fig. 2-6 (Color) Photo *J-V* curves of the QDSCs based on the ZnO nanwires and the branched ZnO nanowires with the SILAR cycle of 9 times. The dashed lines show the dark *J-V* curves.

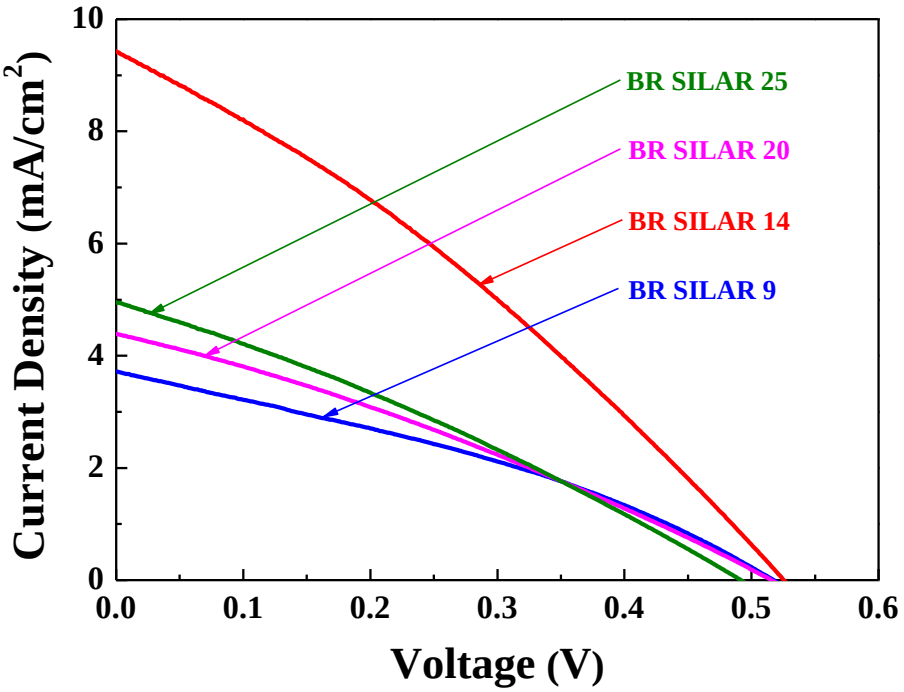

Fig. 2-7 (Color) Photo *J-V* curves of the QDSCs based on the branched ZnO nanwires with different SILAR cycles.

Table 2-1. Solar cell parameters of the QDSCs based on the ZnO nanowires and the branched ZnO nanowires.

	J_{sc} (mA/cm^2)	V_{oc} (V)	*FF*	η (%)
ZnO NW	**2.96**	**0.39**	**0.32**	**0.37**
ZnO BR	**3.72**	**0.52**	**0.33**	**0.64**

Table 2-2. Solar cell parameters of the QDSCs based on the branched ZnO nanowires with different SILAR cycles.

	J_{sc} (mA/cm^2)	V_{oc} (V)	*FF*	η (%)
9 Cycles	**3.72**	**0.52**	**0.33**	**0.64**
14 Cycles	**9.42**	**0.53**	**0.31**	**1.51**
20 Cycles	**4.39**	**0.52**	**0.30**	**0.68**
25 Cycles	**4.95**	**0.49**	**0.29**	**0.72**

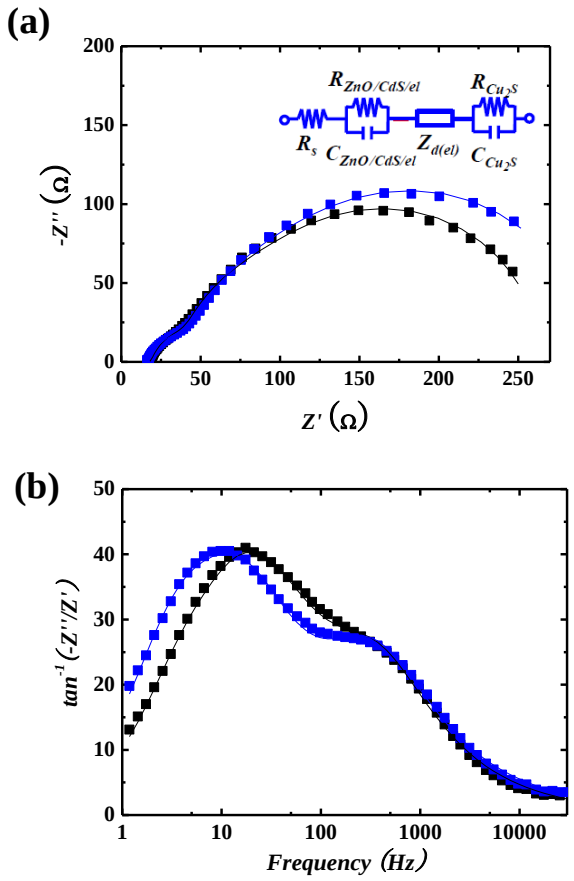

Fig. 2-8 (Color) (a) Nyquist plot and (b) Bode plot of the QDSCs based on the ZnO nanowires and the branched ZnO nanowires, measured under AM 1.5 illumination. The solid line shows the fitted lines.

Table 2-3. Fitting parameters and results of EIS measurement of QDSCs based on the ZnO nanowires and the branched ZnO nanowires.

	ZnO NW	**ZnO BR**
R_S (Ω)	17.7 ± 0.1	15.7 ± 0.1
$R_{ZnO/CdS/el}$ (Ω)	174.0 ± 3.5	185.5 ± 4.6
$C_{ZnO/CdS/el}$ (μF)	223.6 ± 10.0	377.8 ± 20.8
$Z_{d(el)}$-R (Ω)	59.5 ± 3.9	79.0 ± 5.5
$Z_{d(el)}$-T (ms)	19.3 ± 1.5	42.7 ± 3.3
$Z_{d(el)}$-P	0.50 ± 0.08	0.47 ± 0.01
R_{Cu_2S} (Ω)	12.4 ± 0.6	13.2 ± 0.4
C_{Cu_2S} (μF)	50.3 ± 3.2	51.2 ± 2.2

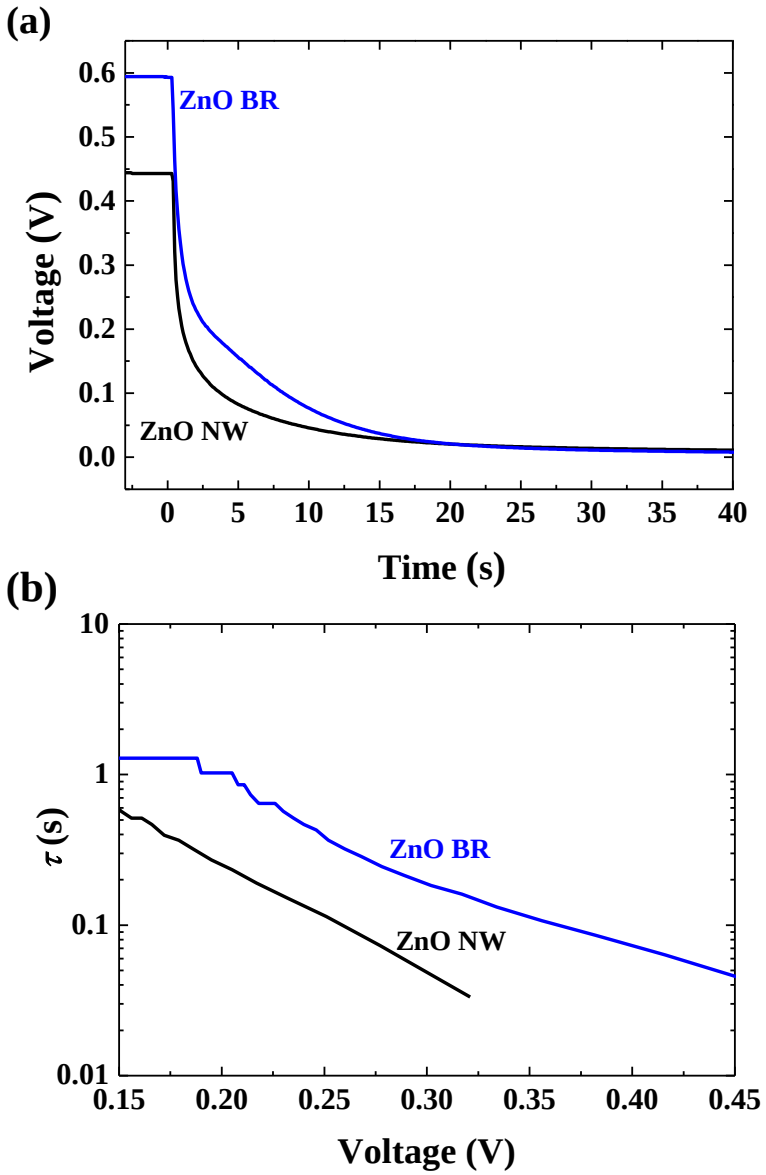

Fig.2-9 (Color) (a) V_{OC}-decay curves of the QDSCs based on the ZnO nanowires and the branched ZnO nanowires. (b) The electron lifetime from Eq. (1) as a function of voltage.

2.4 Conclusion

The branched ZnO nanowires of ~8 μm in length and 100 - 500 nm in diameter were successfully synthesized by a simple hydrothermal method for the photoelectrodes in QDSCs. Primary nanowires provide the direct electron path way, and the secondary nanowires, branches, enlarge the internal surface area for higher QD loading and enhanced light scattering. Both J_{SC} and V_{OC} of branched ZnO nanowires were increased, resulting in the power conversion efficiency (PCE) of 0.64%, which is as twice as that of ZnO nanowires (0.37%). By electrochemical impedance spectroscopy (EIS), the higher charge transfer resistance at ZnO/CdS/electrolyte interface was observed, indicating the retarded back recombination. V_{OC} decay also showed the slower rate and the higher carrier lifetime for the branched ZnO nanowires, which are consistent with the EIS results.

This morphology showed impressive enhancement of both J_{SC} and V_{OC}, even though the optimization of morphology evolution was not achieved. It is expected that further modification of branched morphology and adoption of QDs with lower band gap would enable much higher PCE for QDSC.

2.5 References

1. U. R. Genger, M. Grabolle, S. C. Jaricot, R. Nitschke, and T. Nann, "Quantum Dots versus Organic Dyes as Fluorescent Labels," *Nat. Methods.* **5**, 9 (2008).
2. R. J. Ellingson, M. C. Beard, J. C. Johnson, P. Yu, O. I. Micic, A. J. Nozik, A. Shabaev, and A. L. Efros, "Highly Efficient Multiple Exciton Generation in Colloidal PbSe and PbS Quantum Dots," *Nano Lett.* **5**, 865 (2005).
3. N. Kopidakis, K. D. Benkstein, J. Lagemaat, and A. J. Frank, "Transport-Limited Recombination of Photocarriers in Dye-Sensitized Nanocrystalline TiO_2 Solar Cells," *J. Phys. Chem. B* **107**, 11307 (2003).
4. E. M. Kaidashev, M. Lorenz, H. Von Wenckstern, A. Rahm, H. C.Semmelhack, K.-H. Han, G. Benndorf, C. Bundesmann, H. Hochmuth, and M.Grundmann, "High Electron Mobility of Epitaxial ZnO Thin Films on C-plane Sapphire Grown by Multistep Pulsed-Laser Deposition," *Appl. Phys. Lett.* **82**, 3901 (2003).
5. Z. L. Wang, "Zinc Oxide Nanostructures: Growth, Properties and Applications," *J. Phys.: Condens. Matter* **16**, R829 (2004).
6. Y. Shi, C. Zhu, L. Wang, C. Zhao, W. Li, K. K. Fung, T. Ma, A. Hagfeldt, and N. Wang, "Ultrarapid Sonochemical Synthesis of ZnO Hierarchical Structures: From Fundamental Research to High Efficiencies up to 6.42% for Quasi-Solid Dye-Sensitized Solar Cells," *Chem. Mater.* **25**, 1000 (2013).
7. H. -M. Cheng, W. -H. Chiu, C. -H. Lee, S. -Y. Tsai, and W. -F. Hsieh, "Formation of Branched ZnO Nanowires from Solvothermal Method and Dye-Sensitized Solar Cells Applications," *J. Phys. Chem. C* **112**, 16359 (2008).

8. S. H. Ko, D. Lee, H. W. Kang, K. H. Nam, J. Y. Yeo, S. J. Hong, C. P. Grigoropoulos, and H. J. Sung, "Nanoforest of Hydrothermally Grown Hierarchical ZnO Nanowires for a High Efficiency Dye-Sensitized Solar Cell," *Nano Lett.* **11**, 666 (2011).
9. Q. Zhang, T. P. Chou, B. Russo, S. A. Jenekhe, and G.Cao, "Aggregation of ZnO Nanocrystallites for High Conversion Efficiency in Dye-Sensitized Solar Cells," *Angew. Chem.* **120**, 2436 (2008).
10. H. Kim and K. Yong, "A Highly Efficient Light Capturing 2D (nanosheet)-1D (nanorod) Combined Hierarchical ZnO Nanostructure for Efficient Quantum Dot Sensitized Solar Cells," *Phys.Chem. Chem. Phys.* **15**, 2109 (2013).
11. F. Zhu, H. Dong, Y. Wang, D. Wu, J. Li, J. Pan, Q. Li, X. Ai, J. Zhang, and D. Xu, "Dual-Functional Hetero-Structured TiO_2 Nanotrees Composed of Rutile Trunks and Anatase Branches for Improved Performance of Quantum Dot-Sensitized Solar Cells," *Phys.Chem. Chem. Phys.* **15**, 17798 (2013).
12. C. Xu, P. Shin, L. Cao, and D. Gao, "Preferential Growth of Long ZnO Nanowire Array and Its Application in Dye-Sensitized Solar Cells," *J. Phys. Chem. C* **114**, 125 (2010).
13. H. Lee, H. C. Leventis, S.-J. Moon, P. Chen, S. Ito, S. A. Haque, T. Torres, F. Nuesch, T. Geiger, S. M. Zakeeruddin, M. Grätzel, and K. Nazeeruddin, "PbS and CdS Quantum Dot-Sensitized Solid-State Solar Cells: "Old Concepts, New Results"," *Adv. Func. Mater.* **19**, 1 (2009).
14. Y. -L. Lee and C.-H. Chang, "Efficient Polysulfide Electrolyte for CdS Quantum

Dot-Sensitized Solar Cells," *J. Power Sources* **185**, 584 (2008).

15. J. Kim, H. Choi, C. Nahm, C. Kim, J. I. Kim, W. Lee, S. Kang, B. Lee, T. Hwang, H. H. Park, and B. Park, "Graded Bandgap Structure for PbS/CdS/ZnS Quantum-Dot-Sensitized Solar Cells with a $Pb_xCd_{1-x}S$ Interlayer," *Appl. Phys. Lett.* **102**, 183901 (2013).
16. S. Xu and Z. L. Wang, "One-Dimensional ZnO Nanostructures: Solution Growth and Functional Properties," *Nano Res.* **4**, 1013 (2011).
17. F. Zhao, J. –G. Zheng, X. Yang, X. Li, J. Wang, F. Zhao, K. Sing, W., C. Liang, and M. Wu*, "Complex ZnO Nanotree Arrays with Tunable Top, Stem and Branch Structures," *Nanoscale* **2**, 1674 (2010).
18. R. Vogel, P. Hoyer, and H. Weller, "Quantum-Sized PbS, CdS, Ag_2S, Sb_2S_3, and Bi_2S_3 Particles as Sensitizers for Various Nanoporous Wide- Bandgap Semiconductors," *J. Phys. Chem.* **98**, 3183 (1994).
19. V. González-Pedro, X. Xu, I. Mora-Seró, and J. Bisquert, "Modeling High-Efficiency Quantum Dot Sensitized Solar Cells," *ACS Nano* **4**, 5783 (2010).
20. F. Fabregat-Santiago, J. Bisquert, E. Palomares, L. Otero, D. Kuang, S. M. Zakeeruddin, and M. Grätzel, "Correlation between Photovoltaic Performance and Impedance Spectroscopy of Dye-Sensitized Solar Cells Based on Ionic Liquids," *J. Phys. Chem. C* **111**, 6550 (2007).
21. J. Bisquert, "Theory of the Impedance of Electron Diffusion and Recombination in a Thin Layer," *J. Phys. Chem. B* **106**, 325 (2002).
22. H. Choi, J. Kim, C. Nahma, C. Kim, S. Nam, J. Kang, B. Lee, T. Hwang, S. Kang,

D. J. Choi, Y. -H.Kim*, B. Park*, “The role of ZnO-coating-layer thickness on the recombination in CdS quantumdot- sensitized solar cells,” Nano Energy 2, 1218 (2013).

23. J. Kim, H. Choi, C. Nahm, C. Kim, S. Nahm, S. Kang, D. -R. Jung, J. I. Kim, J. Kang, and B. Park, “The Role of a $TiCl_4$ Treatment on the Performance of CdS Quantum-Dot-Sensitized Solar Cells,” *J. Power Source* **220**, 108 (2012).
24. A. Zaban, M. Greenshtein, and J. Bisquert, “Determination of the Electron Lifetime in Nanocrystalline Dye Solar Cells by Open-Circuit Voltage Decay Measurements,” *ChemPhysChem* **4**, 859 (2003).

국문 초록

ZnO 나노와이어에 2 차 ZnO 나노와이어를 성장시켜 표면적과 광 산란이 우수한 나노구조를 합성하여 CdS 양자점 감응형 태양전지의 광전극으로 활용하였다. 수열 합성법을 통해 1 차원 ZnO 나노와이어에 2 차 나노와이어들이 자란 3 차원 나노트리 구조를 얻었다. 이러한 나노구조는 직선 전자이동 경로를 제공하여, 전자 이동에 유리하고, 양자점이 형성되는 광전극의 표면적이 효과적으로 증가하여 광흡수가 증가한다. 또한 1 차원 나노와이어에 비하여 3 차원 나노구조는 광산란 또한 향상시킴을 관찰하였다. 그 결과로 곡선 인자는 비슷하지만 개방전압과 단락전류가 증가하면서 2 배에 달하는 광변환효율 향상을 보였다. 전기화학적 특성 분석을 통해 2 차 나노와이어의 성장으로 인해 더 많은 ZnO/전해질 계면이 형성됨에도 재결합이 줄어들어 양자점 감응형 태양전지 광전극으로써 우수한 특성을 가짐을 보였다.

***주요어*:** 양자점 감응형 태양전지, ZnO 나노와이어, 나노트리 구조, 광 산란

학번: 2012-20573